Limnol. Oceanogr., 31(6), 1986, 1232–1254

Wind-induced internal seiches in Lake Zurich observed and modeled[1]

W. Horn
Deutsches Hydrographisches Institut, Bernhard-Nocht-Str.78, D-2000 Hamburg, FRG

C. H. Mortimer
Center for Great Lakes Studies, University of Wisconsin–Milwaukee, Milwaukee 53201

D. J. Schwab
Great Lakes Environmental Research Laboratory, NOAA, 2300 Washtenaw Avenue, Ann Arbor, Michigan 48104

Abstract

During August and September 1978, 31 current meters and 120 temperature sensors were deployed to record every 10 or 20 min at various depths at 12 moorings (with wind speed and direction at three moorings) in Lake Zurich. We explore here the baroclinic (internal seiche) response to wind impulses, observed as fluctuations in isotherm depth and current speeds. Those fluctuations and their energy spectra are compared with the predictions of two models fitted to basin topography and to the observed average thermal structure: a two-layered variable-depth (TVD) model developed by D. J. Schwab, fitted to basin topography and incorporating a two-dimensional horizontal grid, and C. H. Mortimer's two-layered modification of a simpler procedure originally developed for surface seiche calculations by A. Defant.

The dominant responses to wind impulses were internal seiches of the first longitudinal mode (average period 44 h). Weaker signals from the second (24 h) and third (17 h) modes were also seen in spectra of temperature and current fluctuations. The models displayed patterns of thermocline displacement and current which, in periodicity and structure, were closely similar to those observed. Predictions of the Defant model were less precise, particularly for current.

Founded on linear theory and neglecting the effects of rotation, the models were unable to reproduce two features occasionally seen in the lake motions: clockwise or anticlockwise rotation of current direction; and internal surges arising when storms induced large-amplitude downstrokes of the thermocline at one basin end or the other. The lake's internal response was principally dependent on the timing, strength, and duration of the wind impulse, relative to and interacting with internal seiche motions already in progress.

We here describe and interpret some features of the internal motion recorded by instruments moored at various depths in the main basin of Lake Zurich (Untersee) during August and September 1978. We are grateful to many individuals for encouragement and critiques, in particular to K. Hutter. We thank C. Bucher for figure preparation and G. Oman for permission to include the output from his model in our Fig. 11. Descriptions of the instruments, the mooring arrangements, and the data processing procedures were given by Horn (1980). Twelve recording stations were established (Fig. 1). Moorings 1 and 12 each consisted of a single current meter at 6-m depth, i.e. above the thermocline, which was present at an average depth of 12 m throughout the 2 months of record. At the other moorings two or more current meters and a thermistor chain with equally spaced temperature sensors were deployed at the depths listed in Table 1. The current meters recorded speed and direction of flow (and some also temperature) every 10 min, and the thermistor chains recorded temperature every 20 min. In addition, moorings 4, 6, and 11 were equipped with separate surface buoys recording meteorological variables, which (significantly for our present purpose)

[1] Contribution 283, Center for Great Lakes Studies; Contribution 473, Great Lakes Environmental Research Laboratory. This work was supported as part of the Swiss National Foundation's 5-year program, "Grundlegende Probleme des Schweizerischen Wasserhaushaltes," and was carried out at the VAW (Versuchsanstalt für Wasserbau, Hydrologie, and Glaziologie) Eidgenossische Technische Hochschule, CH 8092 Zurich.

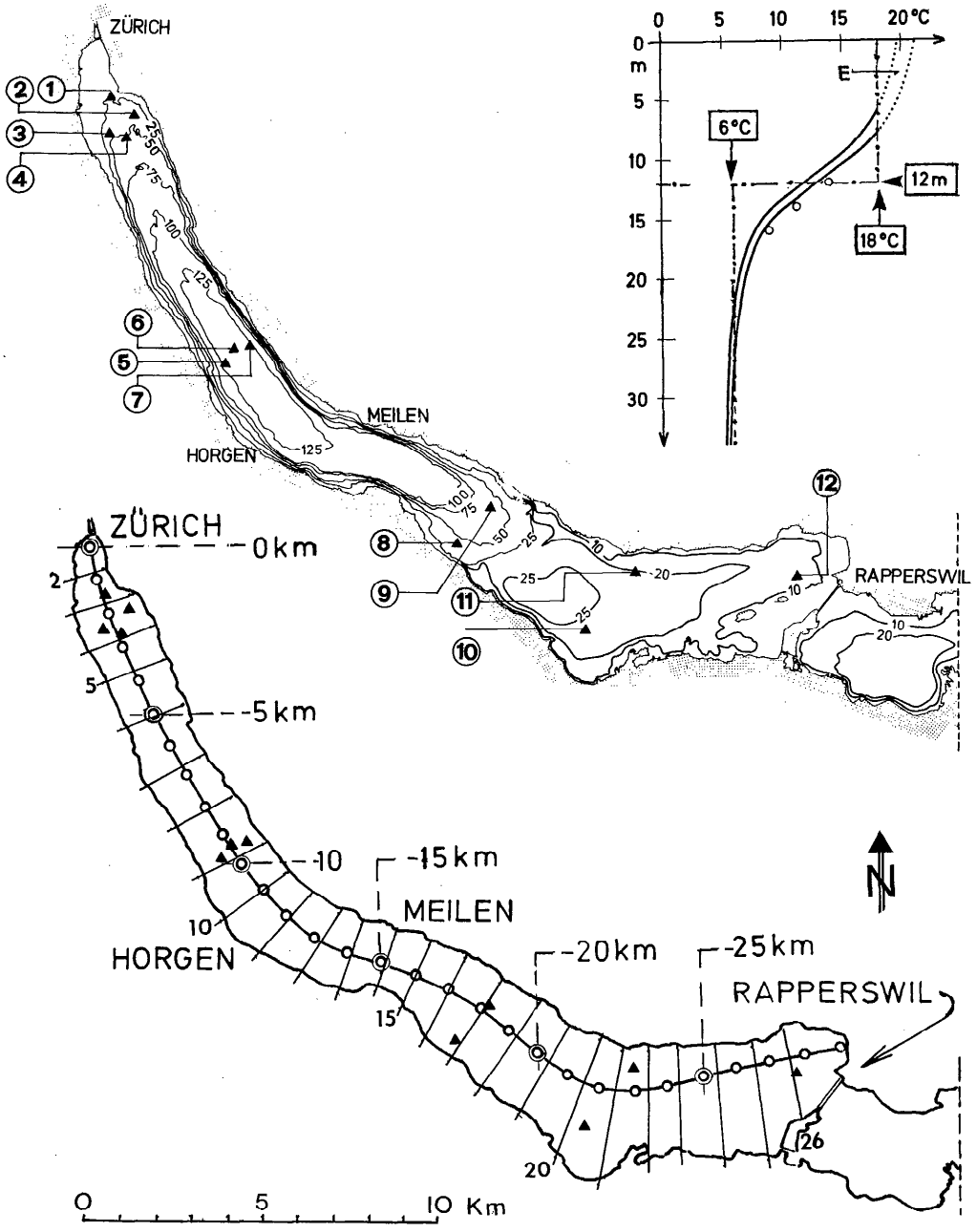

Fig. 1. Bathymetric chart of Lake Zurich; ▲— 1978 positions of current meter and thermistor-chain moorings (1–12, Table 1). Depth contours are in meters, relative to a mean surface level of 406 m ASL; the lower chart displays the cross-sections (2–26) used in the Defant calculation and the Talweg (defined in the text) marked at kilometer intervals (O). Temperature/depth profiles at eleven of the moorings, averaged over the interval 6 August–28 September 1978, fall within the double-line envelope illustrated at the top right (from W. Horn's data report, *see Fig. 2 legend*). Mooring 4 values are shown circled; extrapolation E above 6 m is shown dotted. The two-layered approximation to the whole-basin average profile is displayed by dash-dot lines.

Table 1. Depth and record durations of instruments at the 1978 moorings.

Mooring	Bottom depth (m)	Record duration	Current meter depth (m)	Thermistor spacing* (m)
1	28	3 Aug–21 Sep	6	
2	41	3 Aug–21 Sep	9†	11–31
			37	
3	45	3 Aug–21 Sep	5†	7–27
			38	
4	60	4 Aug–28 Sep	6†	8–28
			30†	
			50	
5	128	7 Aug–22 Sep	7†	9–24
			30	
			54	
			106	
6	136‡	6 Aug–28 Sep	10†	12–32
			34†	
			57	
			104	
			128	
7	132	7 Aug–22 Sep	13	16–31
			37	
			60	
8	46	10 Aug–25 Sep	8†	9–29
			32†	
			39	
9	62	10 Aug–25 Sep	8†	10–30
			32†	
			39	
10	24	10 Aug–25 Sep	7	9–19
			20	
11	22	9 Aug–26 Sep	6	8–18
			19	
12	18	9 Aug–26 Sep	6	

* Eleven, equally spaced over the range shown.
† Aanderaa current meters which also recorded temperature; the others were constructed at VAW (Switzerland).
‡ Maximum depth of the lake.

included wind speed and direction at 3, 4, and 7 m above the water surface.

Displacement of isothermal surfaces from their equilibrium positions in Lake Zurich, during and after wind stress, was observed over 30 years ago by Thomas (1949, 1950) who concluded that internal seiches were generated in that manner. A more comprehensive description and interpretation of the responses of the lake to wind impulses—a long-time interest of the second author (Mortimer 1953)—can now be attempted, with the availability of the 1978 data set for testing simple but adequate interpretative models. To this end, the third author (D.J.S.) has here extended his two-layered constant equivalent depth model (Schwab 1977) to accommodate a more realistic variable-depth bottom layer, neglecting in this case the influence of rotation. The predictions of this model, hereafter called the two-layered variable-depth (TVD) model or TVDM, are here compared with the periodicities and structures seen in the recorded motions and also with results from a simpler, one-dimensional (Defant 1918) procedure, adapted to the two-layered case by Mortimer (1979).

The Untersee basin of Lake Zurich is narrow relative to its length and is divided into three regions (Fig. 1): a deep portion (max depth 136 m) trending generally NW; a transition zone with mean bottom slope of about 3%; and a wider shallower region of mean depth 22 m and trending EW. The average depth of the whole Untersee is 51 m, its area 67 km^2, and the Talweg track (a smoothed curve following the deepest contours of the channel) is 30 km long (28 km along the interface, Fig. 1).

Changes in the Talweg direction along the basin and the varied topography of surrounding landforms impose a marked variability and nonuniformity on the distribution of wind stress on the water surface and on the subsequent responses of the water masses. Nevertheless, the most common immediate internal response to wind stress is a tilt imposed on the thermocline and directed along the Talweg channel. The topography of that channel also guides the propagation of the long internal waves which follow the disturbance. Inspection and spectral analysis of both temperature and current records show that the subsequent response is a combination of several internal seiche (standing wave) modes, the first being dominant. Those oscillations persist with diminishing amplitude until equilibrium is restored or is again disturbed by a new wind impulse. Their frequencies and structures are satisfactorily simulated by the TVD model and also, less closely, by the Defant model. Features not reproduced in the models—rotations in current direction, generation of internal surges when seiche amplitudes become large—are briefly described in the concluding section.

Internal seiche responses to wind impulses; variation in wind stress and isotherm depth, August–September 1978

The basic data set for water temperature comprises readings at moorings 1–12 every 10 min at current meter depths and every 20 min at thermistor depths over the nearly 2-month intervals listed in Table 1. Plots of temperature at each mooring and depth were assembled in a comprehensive data report, from which Fig. 2 is a sample extract. From such records we have prepared, by linear interpolation, plots of hourly averaged isotherm depth for the whole recording interval at each mooring except 1 and 12. In Fig. 3, the depth variation of the 10°C (a midthermocline) isotherm at mooring 4 near the NW end of the basin is compared with its counterpart at mooring 11 near the SE end. Also compared are the depth fluctuations of the 10°C isotherm at moorings 6 and 9 in the central region of the basin and the hourly averaged EW and NS components of wind speed squared (approximately proportional to wind stress) at 3 m above the lake surface at moorings 6 and 11.

Inspection of Fig. 3 leads us to conclude the following:

- The wind stresses on the lake were relatively weak for most of the period except for a group of wind impulses from 30 August to 2 September and a strong storm on 11–12 September, during which the eastgoing wind component at mooring 6 reached a maximum hourly mean speed of 9.6 m s^{-1}. The lake's response to that storm was dramatic; the depth fluctuations of the 10°C isotherms at moorings 4 and 11 exceeded the respective measuring ranges of the thermistor chains. On this and other occasions, the fluctuations in isotherm depth were greater near the ends of the basin (at moorings 4 and 11) than near the middle (at moorings 6 and 9), and the record pairs (4/11 and 6/9) more often than not showed antiphase behavior, particularly during intervals of relatively regular oscillation. This behavior is consistent with the relative positions of the moorings and an amplitude distribution dominated by the first internal basin mode.

- Until 30 August the winds were very weak; nevertheless some periodic responses with an average periodicity close to 44 h—fitted visually in the figure and consistent with dominance of the first mode with the deflections at 4 and 11 out of phase—can be seen in the 25–28 August example (▲). Corresponding antiphase behavior at the same average periodicity is also visible in the 24–27 August records from moorings 6 and 9. However, that oscillation appears to have been interrupted at all four moorings on 30 August, probably as a result of an eastgoing wind impulse on that day.

- Although the first modal (44 h) response is the most conspicuous, occasional evidence of an oscillation of period near 24 h also is seen in Fig. 3. For example, the open triangles and vertical arrows (15–25 August, 31 August–8 September) demonstrate antiphase relationships between isotherm deflections at moorings 4 and 9, shown below to be consistent with a second mode response. The fact that no consistent relationship with mooring 6 is visible is probably a consequence of the location of that mooring near a binodal point (cf. Fig. 4).

- At the end of the interval of variable winds (30 August–2 September) a series of near-44-h oscillations persisted, generally showing the isotherm deflections at moorings 4 and 11 to be in antiphase and increasing in amplitude up to 10 September. A similar antiphase relationship between the deflections at moorings 6 and 9 also appeared during 9–10 September, which may have been the result of weak winds (7–9 September) which followed a 3-day interval of calm weather. That oscillation was then further amplified by the strong eastgoing wind impulse on 11–12 September, the timing of which apparently fell nearly in phase with, and therefore reinforced, the pre-existing (first-mode) oscillation.

- During the calm interval (13–15 September) after the storm, the near-44-h oscillation was damped relatively rapidly; it was (apparently) also disturbed by the wind impulses of 18–19 September. Unlike other lakes in which the dominant first internal mode response persists for many oscillation cycles (Mortimer 1953), Lake Zurich ap-

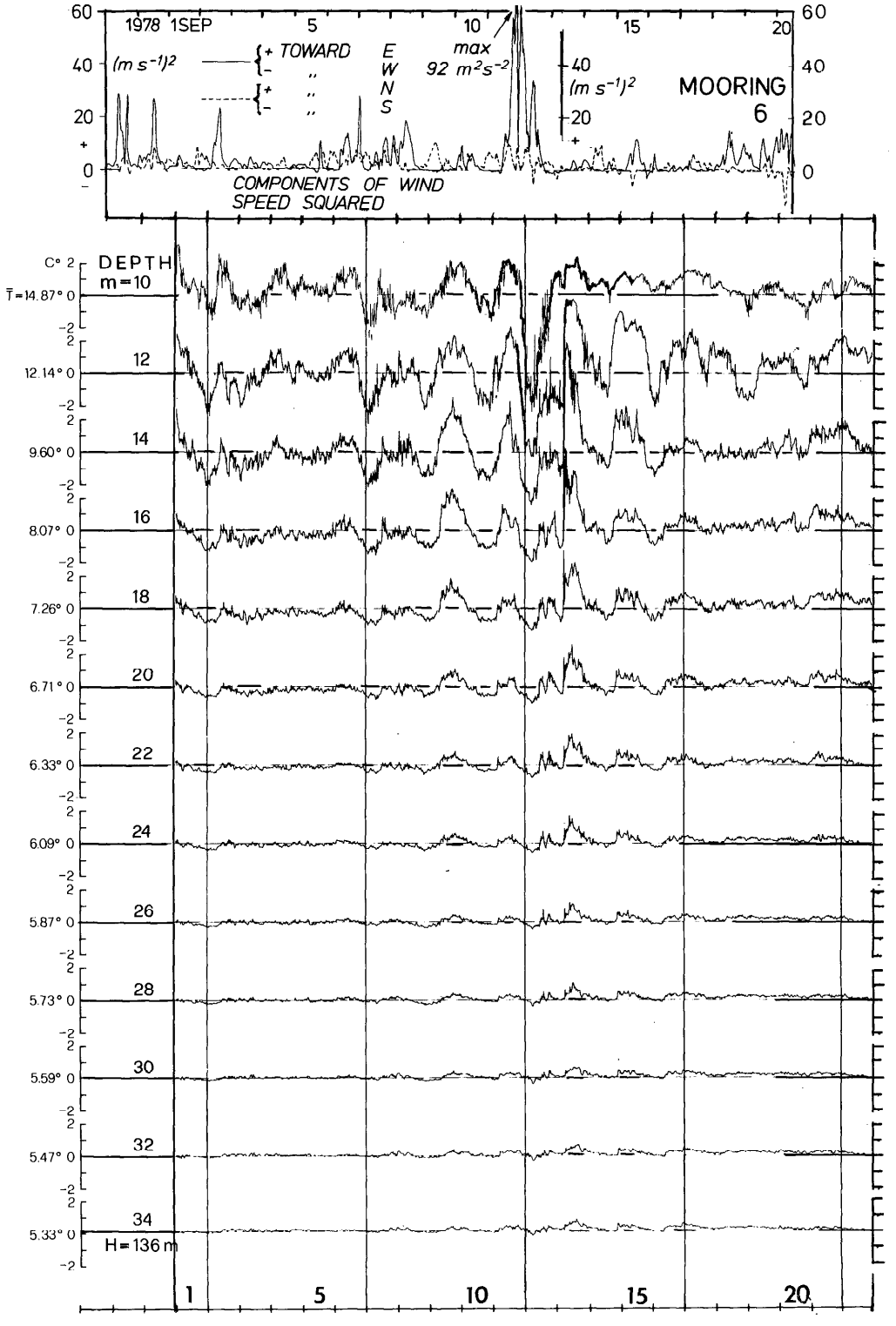
1978 1SEP
5
10
15
20
60
40
20
0
(m s⁻¹)²
+ TOWARD
E
W
N
S
max
92 m²s⁻²
40
20
(m s⁻¹)²
MOORING
6
COMPONENTS OF WIND
SPEED SQUARED
C° 2
DEPTH
m=10
T̄=14.87° 0
12
12.14° 0
14
9.60° 0
16
8.07° 0
18
7.26° 0
20
6.71° 0
22
6.33° 0
24
6.09° 0
26
5.87° 0
28
5.73° 0
30
5.59° 0
32
5.47° 0
34
5.33° 0
H=136 m
-2
1
5
10
15
20

pears to be subject to a relatively high rate of frictional damping, perhaps engendered by the extensive shallow shelf at the SE end of the basin.

The above conclusions, drawn from visual inspection of the records and confirmed and extended by later spectral analysis, will now be compared with the predictions of models in which the observed average temperature structure is replaced by a two-layered one.

The models and their predictions

The two-layer variable-depth (TVD) model—To model the observed internal free oscillations in Lake Zurich, we represent the stratification by a two-layer approximation with an upper layer of density ρ_1 and a lower layer of slightly greater density ρ_2. As a first approximation, rotation of the earth is neglected. The linearized equations of motion in this case become

$$i\sigma \mathbf{v}_1 = -g\nabla(\eta + \eta_2) \quad (1)$$

$$i\sigma\eta = -\nabla \times (h_1\mathbf{v}_1) \quad (2)$$

$$i\sigma \mathbf{v}_2 = -g\nabla(\delta\eta + \eta_2) \quad (3)$$

$$i\sigma\eta_2 = -\nabla \times (h_2\mathbf{v}_2). \quad (4)$$

Here σ is the frequency of oscillation; $\mathbf{v}_1$ and $\mathbf{v}_2$ are the upper- and lower-layer horizontal velocity vectors; $\eta = \eta_1 + \eta_2$, in which η_1 is the free surface displacement, η_2 is the interface displacement; h_1 and h_2 are the upper- and lower-layer equilibrium depths (or thicknesses); g is the gravitational constant; ϵ (*see Eq. 9*) is the relative density difference between the upper and lower layers [$\epsilon = (\rho_2 - \rho_1)/\rho_2$]; and $\delta = 1 - \epsilon$. Both layers are assumed to extend all the way to a vertical wall at the shoreline so that the boundary conditions at the shoreline are

$$\mathbf{v}_1 n = 0, \quad \mathbf{v}_2 n = 0 \quad (5)$$

and

$$\frac{\partial\eta}{\partial n} = 0, \quad \frac{\partial\eta_2}{\partial n} = 0 \quad (6)$$

in which n denotes a unit normal vector.

In this lake the internal Rossby radius of deformation is about the same as the width of the lake, so that the approximation of no rotation is not completely justified. The lowest longitudinal internal modes appear to have some of the characteristics of Kelvin waves in a rotating channel, and evidence of this is seen when temperature records from mooring pairs 5/7 and 8/9 are compared. The main effect of rotation is to bring about a transverse slope of the interface which generates a pressure gradient in approximate geostrophic balance with the longitudinal current, as in the Loch Ness example (Mortimer 1955). The frequency, to a first approximation, is unaffected. Those effects, not included in the TVDM predictions, must be borne in mind when the model results are examined.

Equations 1 and 3 can be used to eliminate the velocity vector from Eq. 2 and 4, so that

$$-\sigma^2/g\eta = h_1\nabla^2(\eta + \eta_2) \quad (7)$$

and

$$-\sigma^2/g\eta = \nabla \times h_2\nabla(\delta\eta + \eta_2). \quad (8)$$

Equations 7 and 8 are made discrete on a rectilinear grid (of n 0.5-km squares, Fig. 4) replacing the spatial derivatives with centered differences. Areas of the lake shallower than 12 m have been eliminated from the grid, which was based on one with 250-m squares constructed by Oman (1982) for a multilayered wind-driven circulation model of the lake. The resulting 2n × 2n standard eigenvalue problem, solved with routines described by Smith et al. (1974), yields eigenvalues of $-\sigma^2/g$ and eigenvectors con-

←

Fig. 2. Extract from W. Horn's data report, "Zürichsee 1978" (deposited at VAW, *see footnote 1*) presenting temperature (°C) records at 13 depths at mooring 6, Lake Zurich, 1–22 September 1978, GMT, plotted as deviations from the 6 August to 28 September means listed in the left-hand column. The top panel displays the EW and NS components of wind speed squared, 3 m above lake surface at mooring 6.

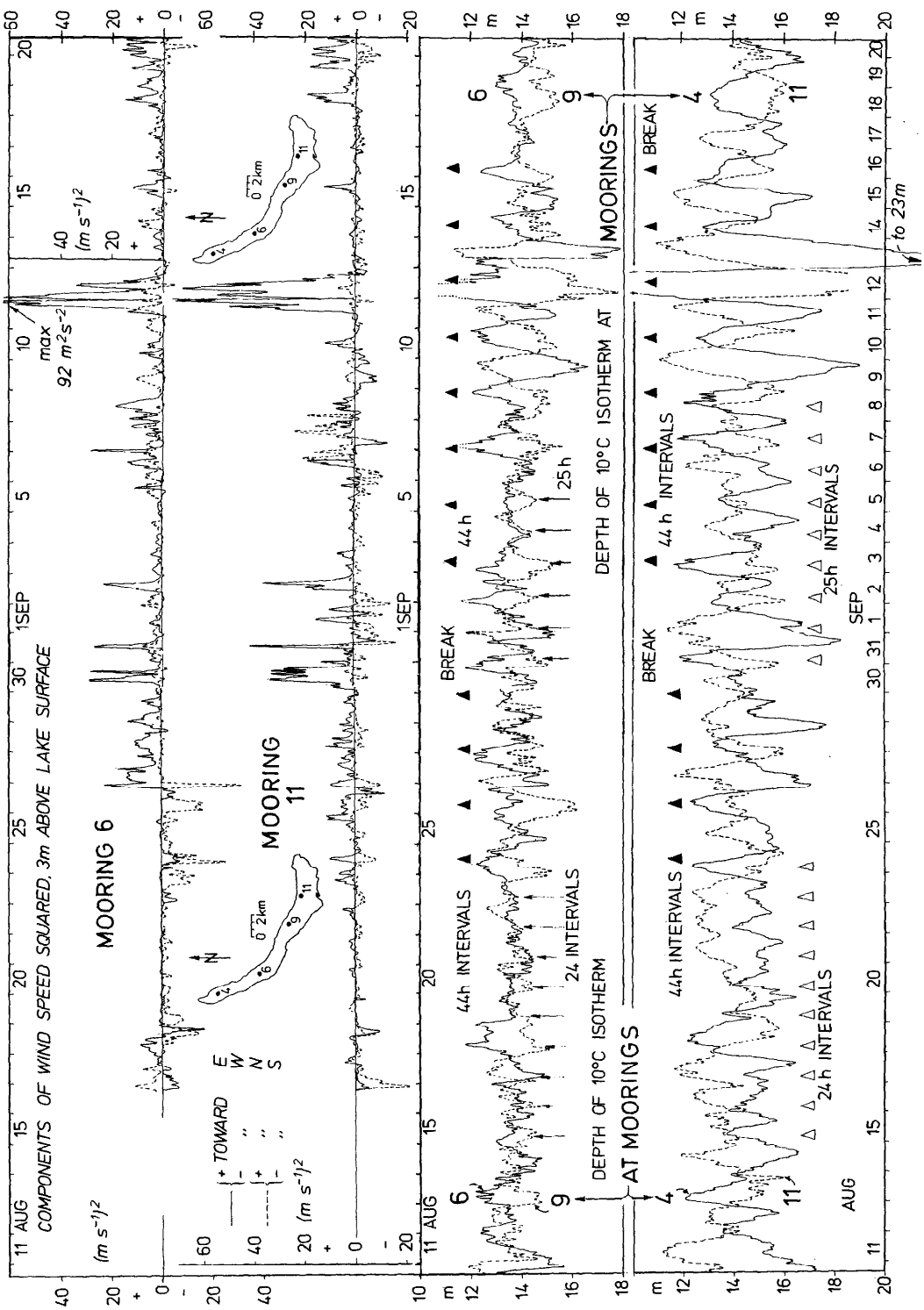
COMPONENTS OF WIND SPEED SQUARED, 3m ABOVE LAKE SURFACE
(m s⁻¹)²
MOORING 6
MOORING 11
+ TOWARD E
− " W
+ " N
− " S
(m s⁻¹)²
max 92 m²s⁻²
(m s⁻¹)²
0 2km
11 AUG
1SEP
SEP
AUG
BREAK
44h INTERVALS
24h INTERVALS
25h INTERVALS
24 INTERVALS
DEPTH OF 10°C ISOTHERM
AT MOORINGS
DEPTH OF 10°C ISOTHERM AT MOORINGS
to 23m
m

sisting of the corresponding η and η_2 fields. The velocity fields for a particular eigenmode can then be constructed with Eq. 1 and 3. (For an application to Lake Lugano, *see* Hutter et al. 1983.)

Application of the TVDM to Lake Zurich requires specification of the upper- and lower-layer densities and equilibrium interface depth. Figure 1 shows the envelope of the mean (August/September) temperature profile for all moorings, to which is fitted the two-layered approximation with 18°C and 6°C as the respective upper- and lower-layer temperatures and with 12 m as the equilibrium depth of the interface (model thermocline). The resulting relative density difference $\epsilon(\rho_2 - \rho_1)$ is 1.306×10^{-3}.

The corresponding periods of the 10 lowest eigenmodes calculated by the TVDM are given in Table 2. The thermocline displacement fields (relative to a maximum of 100 cm) for the first three modes are shown in Fig. 4; the corresponding upper- and lower-layer velocity fields are illustrated in Fig. 5.

An estimate of the periods, which the model would predict if other values of layer density and thickness were chosen, is given by the following approximate formula. If P_{am} is the period predicted for mode number m, using particular values of the relative density difference ϵ_a and equivalent depth h^*_a, where $h^*_a = h_1h_2/(h_1 + h_2)$, then the corresponding period P_{bm} which the model would predict using other values, ϵ_b and h^*_b, is given to a close approximation by

$$P_{bm} = P_{am}[(\epsilon_a h^*_a)/(\epsilon_b h^*_b)]^{1/2}. \quad (9)$$

If, in the present example, the upper-layer temperature had been taken as 20°C instead of 18°C, leaving the other parameters unchanged (Fig. 1), the periods in Table 2 would all be reduced by 13%. On the other hand, the period entries in Table 2 would be increased by 6% if the thickness of the upper layer were reduced from 12 to 11 m while the other parameters are left unchanged. In general, Eq. 9 shows that, within the range of plausible model fittings to the temperature profile in Fig. 1, the calculated periods are more sensitive to changes in the upper-layer temperature than to changes in the other parameters. The mode structures (interface displacements in Fig. 4) are not affected by the period changes in the above hypothetical examples, but the calculated velocities must be multipled by P_{am}/P_{bm}. Thus in the example cited above, in which upper-layer temperature was raised from 18° to 20°C, the velocities displayed in Fig. 5 must be increased by 13%.

The interface displacement distributions predicted by the TVD model in Fig. 4 show that the maximum deflection occurs at the Zurich end of the basin for the first mode, but at the Rapperswil end for the second and third. There is a region about halfway along the basin (not occupied by moorings) in which the deflection contributions of the first and third modes are small (i.e. in the neighborhood of the nodal lines), but the second mode contribution is substantial.

Figure 5 illustrates, for the first three internal modes, the influence of basin topography on the maximum current fields in the upper and lower layers. Generally, as expected, the highest velocities are found in nodal regions, and the lower-layer currents are generally less than (and always opposed in direction to) those in the upper layer. Exceptions occur in the shallow parts of the basin (particularly near Rapperswil in the second and third mode cases) where the thickness of the lower layer becomes less than that of the upper layer and, consequently, the currents are fastest in the lower layer. Although the current fields were calculated with the same maximum interface deflection (100 cm) for each mode, the region of fastest current is much more extensive for the first mode (upper layer) than for the other two.

The Defant model—As already noted, the

←

Fig. 3. Wind speed squared (hourly averaged EW and NW components 3 m above the lake surface at moorings 6 and 11) and fluctuations in isotherm depth in Lake Zurich, 11 August–20 September 1978, GMT. The fluctuations in hourly averaged depths of the 10°C isotherms are interpolated from temperature records at fixed depths at moorings 4, 6, 9, and 11. The September portion of this record was illustrated and discussed elsewhere (Mortimer and Horn 1982).

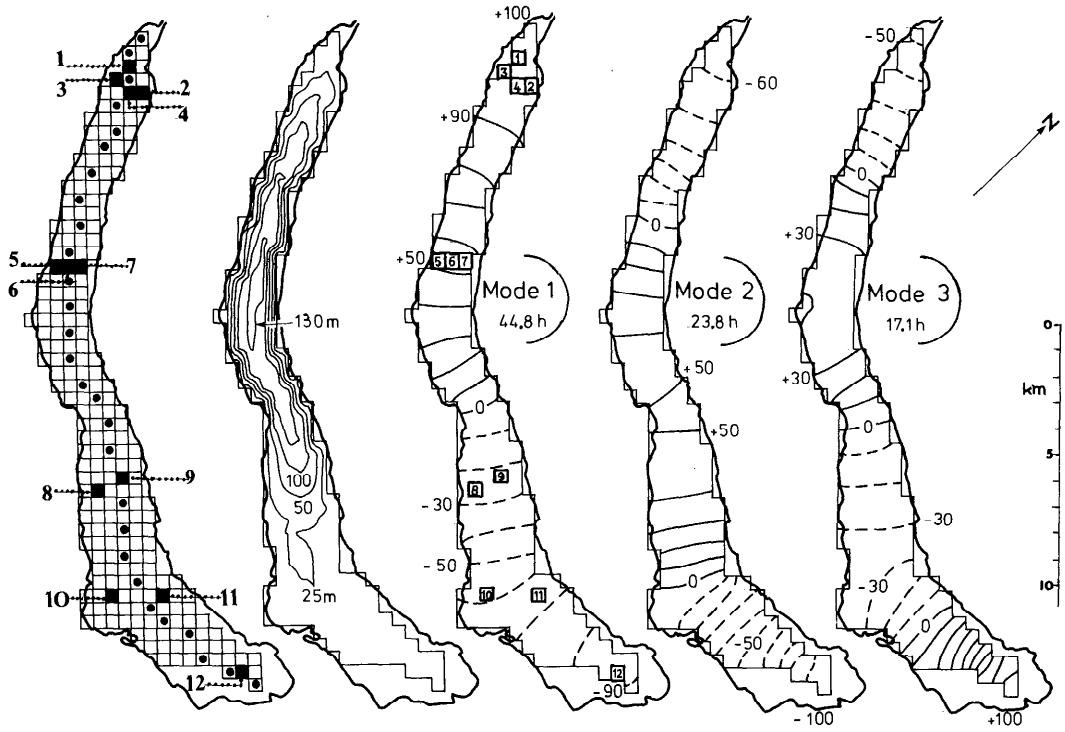

Fig. 4. Predictions by the TVDM of interface elevation distributions, associated with the first three internal modes, relative to a maximum elevation of 100 in each case and with upper- and lower-layer temperatures and interface depth as defined in Fig. 1, top right. The model grid (based on a design by Oman 1982) and the corresponding model depth contours are shown at the left. ■—Mooring positions 1–12; ●—grid-points taken to represent the Talweg for comparisons with the Defant model.

topographically steered seiche currents generally follow the local trend of the Talweg (●—Fig. 4). Using the Talweg as the axis, Defant (1918) devised a simple, one-dimensional procedure for calculating the periods and structures of *surface* seiche modes, which gave excellent results in relatively regular lake basins. For calculation of the periods and structures of *internal* seiche modes in Lake Geneva, Mortimer (1979) introduced a two-layered modification of Defant's procedure. In the form of a simple computer program, that procedure was tested (Lemmin and Mortimer 1986) in eight lake basins for which adequate observations were available and for which a two-layered approximation to the density distribution was justified. In tests for Lake Zurich, the Defant predictions were compared with the here-predicted along-Talweg distributions (Figs. 4 and 5) of interface elevation and maximum current speed and with relative "observed" seiche amplitudes at various moorings, derived from the spectra as described below. (For details of those comparisons *see* Lemmin and Mortimer's figure 8 and related discussion.) Here it suffices to note that, for an interface equilibrium depth of 12 m, layer temperatures of 18° and 6°C,

Table 2. Period of the lowest 10 internal normal modes of Lake Zurich predicted by the TVDM with input parameters defined in the text.

Mode	Period (h)
1	44.8
2	23.8
3	17.1
4	13.4
5	10.6
6	9.5
7	8.2
8	7.2
9	6.7
10	6.1

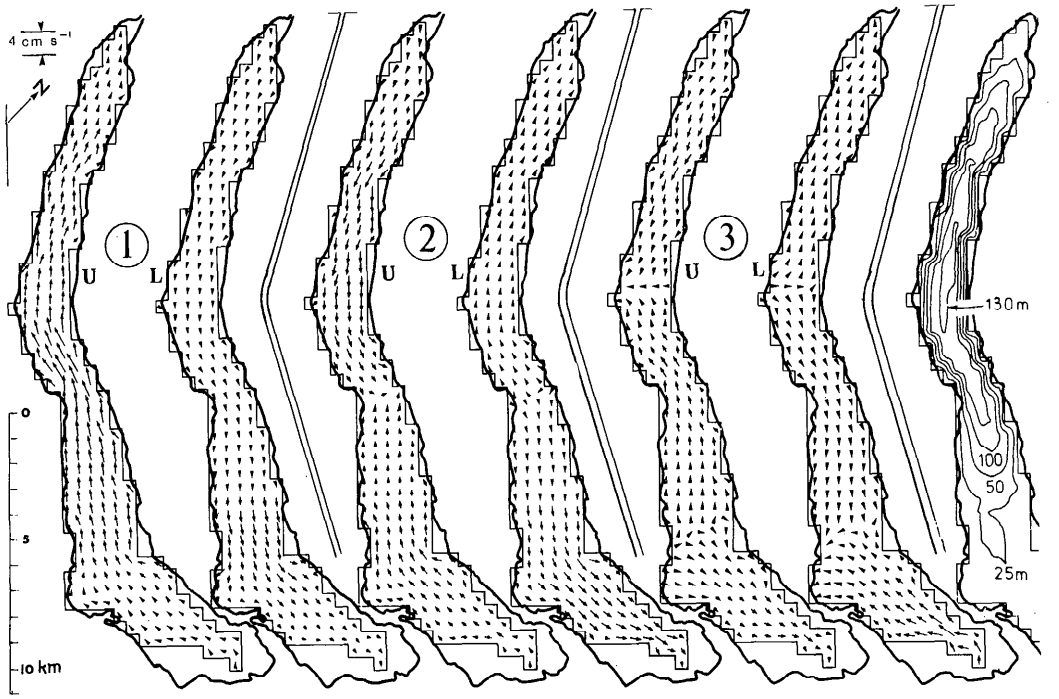

Fig. 5. TVDM-predicted current vectors in the upper (U) and lower (L) layer corresponding to the internal seiches of modes 1, 2, and 3, the elevation distributions of which are illustrated in Fig. 4 (respective periods 44.8, 23.8, and 17.1 h). Vector lengths indicate maximum velocities (speed scale, top left), attained in each case one quarter-period after the elevation maximum. TVDM bathymetry is included (at right) for comparison.

and an interface Talweg terminated by the cross-sections 2–26 (Fig. 1), the Defant-predicted periods for the first three modes were 40.3, 21.3, and 15.2 h, about 10% less than those predicted by the TVDM.

The deflection patterns and nodal positions predicted by the two models are similar; the agreement in predicted amplitude is close for the first mode, but becomes less so as mode number increases. The Defant-predicted current speeds are, in the case of modes 1 and 2, less than those predicted by the TVDM, not surprising because the former are estimated as *averages* for each cross-section, while the TVDM values are calculated for the Talweg grid points where speeds are above the section average. Our general conclusion (confirmed for other basins by Lemmin and Mortimer 1986) is that, despite the necessary assumptions, the simple, one-dimensional Defant procedure can provide useful approximate results with relatively little effort. This was also found to be the case (Lammel 1984) in the less elongated Kochelsee.

Interpretation of spectra

Spectra of temperature fluctuations—Although it is evident from inspection of Fig. 3 that most of the energy associated with temperature fluctuations is concentrated near the TVDM-predicted first and second mode periods (as is also the case for currents), more information is revealed by spectra (prepared by W.H.). The techniques of spectral analysis are well known (Blackman and Tukey 1958; Jenkins and Watts 1968; lake seiche applications in Mortimer and Fee 1976 and Hutter et al. 1983), and only a brief summary of the procedure need be given here. All spectra were prepared from the complete 2-month data sets, consisting of 3,000 20-min readings of temperature (or the u and v components of current or wind). After hourly averaging, each series was divided into three overlapping sections and

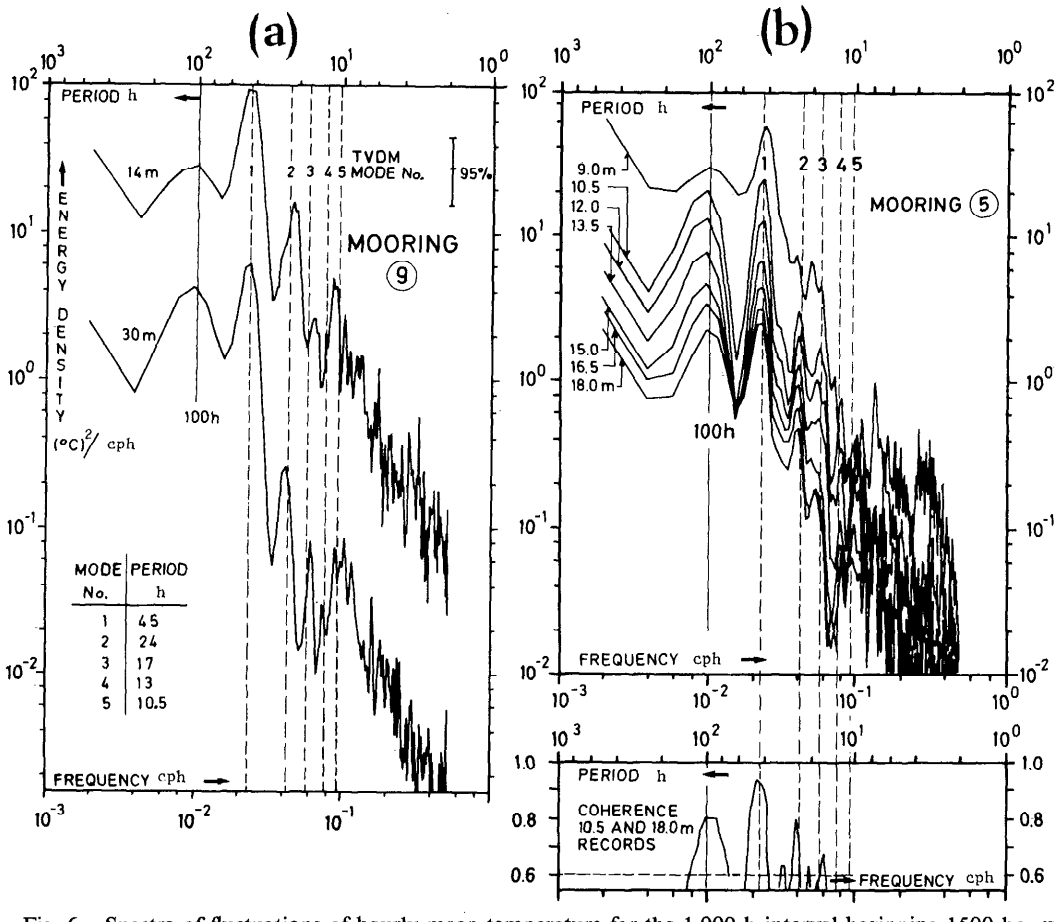

Fig. 6. Spectra of fluctuations of hourly mean temperature for the 1,000-h interval beginning 1500 hours GMT on 10 August 1978: a—at 14- and 30-m depth at mooring 9; b—at seven depths (1.5-m spacing) at mooring 5 (7 August–22 September) plotted on common scales. The lower portion of panel b also displays the frequency distribution of coherence between temperature records from 10.5 and 18 m at mooring 5. In this and later figures, the TVDM-predicted periods for the first five internal (two-layer) modes are indicated by vertical broken lines; the 95% C.I. is a measure of the statistical significance of individual spectral estimates.

further smoothed to improve spectral resolution and statistical confidence in the low frequency region. After Fourier analysis, the computed coefficients were smoothed by standard procedures, optimized by means of test series, yielding normalized spectral estimates of energy density as temperature fluctuations, $(°C)^2$ cph^{-1}, or (for currents or wind) as kinetic energy of the u (EW) or v (NS) components, cm^2 s^{-2} cph^{-1}. The rotary features of the current patterns will be explored later.

Analysis was extended not only to include the autospectra of records from individual moorings and depths as described above, but also to display the coherence and phase relationships between selected data, for example records from pairs of moorings or from pairs of depths at the same mooring.

Representative temperature spectra derived from records obtained near and well below the thermocline (14 and 30 m at mooring 9) are presented in Fig. 6a, in which vertical broken lines denote the TVDM-predicted periods of the first five internal modes (rounded off to the nearest half hour). With a frequency band resolution of 0.00195 cph, the two highest estimates of spectral energy density coincide with the periods 42.7 and 46.5 h. The 45-h line lies within that

band, which evidently displays a dominant first mode response. The energy density at 30 m is <10% that at 14 m, because at 14 m the temperature gradient is much higher (*see Fig. 1*). The highest spectral density estimates near the 24-h (second mode) line lie at 23.3, 24.4, and 25.6 h. Coincidence between conspicuous spectral peaks and the higher mode lines is lacking in Fig. 6a and in most of the spectra illustrated later, demonstrating that modes higher than the third are not appreciably excited.

Cross-spectral analysis (not shown in Fig. 6) of the 14- and 30-m records at mooring 9 discloses significant coherence and an in-phase relationship for the first mode only. Similar in-phase and highly coherent behavior at the 45-h period (less so at 24 h) is seen (Fig. 6b, bottom right) when spectra of records from several depths traversing the thermocline at one mooring are compared. This demonstrates that the vertical structure of the internal wave in this case is dominated by a response in the first vertical mode, with isotherm-depth fluctuations nearly in phase at all depths, and justifies our choice of a two-layered model.

A conspicuous feature of the spectra in Fig. 6, and also of several spectra of temperature and current records illustrated later, is the broad peak centered approximately at a period of 100 h, separated by an energy valley from the first mode peak at 45 h and exhibiting high interdepth coherence. Similar peaks in the 4–5-day period interval, often seen in spectra from other lake records, have been interpreted as the consequence of meteorological forcing associated with the average frequency of weather-front passages. However, the spectrum of wind energy at mooring 6 (not illustrated) shows no large peak in the 4–5-day region. This suggests that the 100-h signal in Lake Zurich may perhaps be a response at a higher vertical mode or a topography-related vorticity wave of the type (and frequency) observed by Saylor et al. (1980) in Lake Michigan. Whether such waves can be important in basins as small as Lake Zurich remains to be explored (Stocker and Hutter 1985). Mysak et al. (1985) presented the first evidence in support of such an occurrence in Lake Lugano.

The dominance in the spectra of the near-45-h peak displays the dominance of the large first mode response, already evident in Fig. 3. If (as will be shown later) the amplitude of that response becomes large, nonlinear features appear as steep-fronted internal surges, with the consequence that harmonic peaks at periods 45/2 and 45/3 h are added to the spectra. The first of such surge harmonics (22.5 h) would contribute to a near-24-h peak (as may also any response to diurnal periodicity in wind stress) making the unambiguous detection of a second basin mode response more difficult. It must also be borne in mind, in any interpretation of spectra of temperature fluctuations, that the variance depends not only on vertical motions, but also on the shape of the vertical temperature gradient at the sensor (*see* discussion by Phillips 1971). Inferences concerning vertical motions should preferably, therefore, be drawn from spectra of isotherm-depth oscillations derived from sensors closely spaced over the vertical range of interest. However, in contemporary spectra of temperature fluctuation and isotherm motion (Fig. 7a), the frequencies, forms, and relative amplitudes of the principal peaks (at 100, 45, 24, 17 h) are similar. It is in the higher frequency range that marked differences appear.

Therefore, if we confine our comparisons to the first and second mode and compare the square roots of peak heights in spectra of temperature or isotherm depth fluctuations at a midthermocline depth (e.g. 13 or 14 m in Fig. 7b), it is possible to obtain approximate estimates of *relative* amplitudes of the internal seiche at moorings spaced along the channel axis and averaged over the 2-month record. Those relative amplitude estimates, deduced for the first mode from the upper row of spectra in Fig. 7b, are 100, 44, 46, and 74 at moorings 4, 6, 9, and 11, respectively. Those amplitude estimates (for the second mode also) are included as vertical lines in Lemmin and Mortimer's (1986) figure 8a. The agreement with the model predictions may be rated as fair for the first mode; the TVDM predicts interface amplitude directly, while the vertical lines represent indirect approximates derived from temperature fluctuations, which

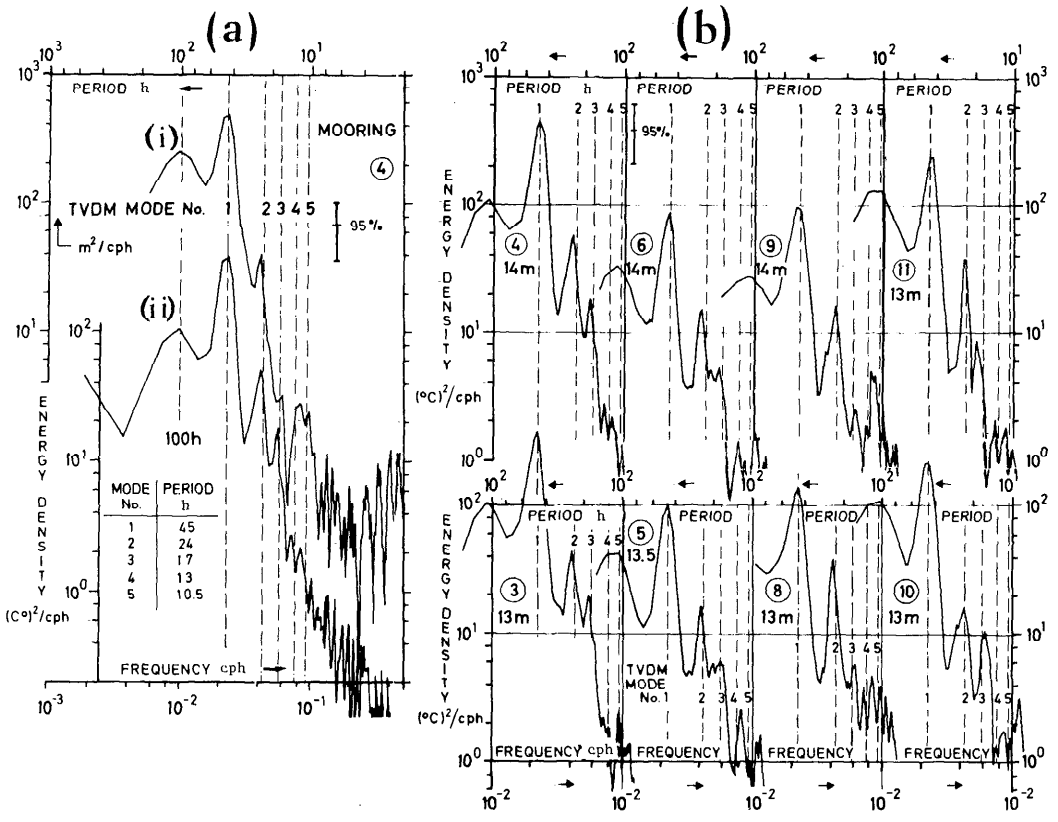

Fig. 7. a. Comparison between spectra of (i) fluctuations in depth of the 12°C isotherm (interpolated from the temperature records) and (ii) recorded fluctuations in temperature at near-thermocline depth (14 m) at mooring 4 (8 August–28 September 1978). b. Spectra of temperature fluctuations at fixed, near-thermocline depths, 10 August–21 September 1978, displayed on a common energy and frequency scale for two sets of moorings (circled numbers) arranged in order along the Talweg.

are proportional to interface-depth fluctuation only in the unlikely event that the vertical temperature gradient was the same at each of the four sensors. The relative heights of the near-45-h peaks at different moorings are probably also influenced by the occasional passage of internal surges; that effect is probably most significant at moorings near the uninode, where isotherm deflection arising from the seiche wave is relatively small compared to that arising from the surge.

Correspondingly normalized estimates of second mode temperature amplitudes at the same four Talweg moorings, proportional to the square roots of the near-24-h peak heights in Fig. 7b, show poor agreement with the TVDM prediction. A possible reason for this—contamination with a 45/2-h harmonic arising from nonlinearity of a large-ampitude seiche or from diurnal fluctuations in wind stress—was mentioned above. Support for this conjecture comes from cross-spectral analysis, which displays coherence and phase relationships between records at the same depth at selected mooring pairs, e.g. 6 and 8 in Fig. 8a. For the dominant near-45-h peak, the coherence for that pair is very high and the phase angle is 150°, i.e. nearly out of phase and consistent with the predicted position of the nodal line in Fig. 4. But for the near-24-h peak the intermooring coherence is very low; we conclude that the moderately large near-24-h peaks in the two spectra are produced by different (and therefore noncoherent) mechanisms. Substantial height differences also

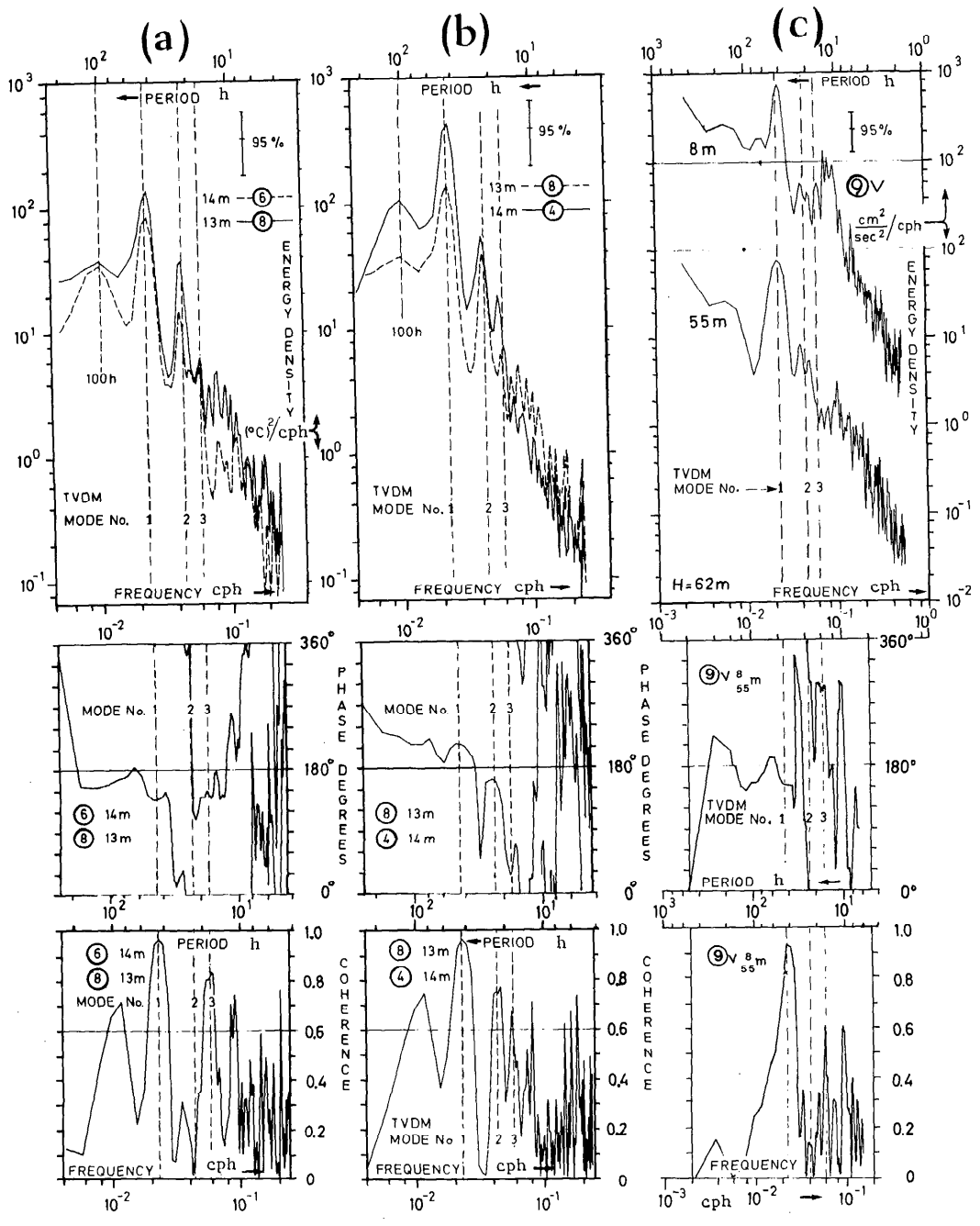

Fig. 8. Spectra of energy, phase angle, and coherence for selected pairs of records, 10 August–21 September 1978: a—temperature fluctuations at near-thermocline depths at the mooring pair 6 and 8; b—the same for mooring pair 8 and 4; c—kinetic energy spectra of the *v* (NS) component of current at 8- and 55-m depths (respectively above and below the thermocline) at mooring 9. A phase angle of 0° or 360° (middle row) at a particular frequency denotes an in-phase relationship; 180° denotes an out-of-phase relationship at that frequency. Coherences are considered *significant* above the 0.6 level.

are sometimes seen in the near-24-h peaks at neighboring moorings (8 and 9, 10 and 11 in Fig. 7b).

Figure 8a also displays moderately high coherence and an out-of-phase relationship for the 17-h presumed third mode peak, consistent with the fact that only one nodal line lies between moorings 6 and 8 (Fig. 4). In another example (mooring pair 4 and 8, Fig. 8b) coherence is again very high near 45 h but differs from the previous example (Fig. 8a) in showing moderately high coherence near 24 h. Coherence is less but still significant near 17 h. The phase differences for the presumed modes 1, 2, and 3 are 210°, 160° (i.e. nearly out of phase), and 20° (nearly in phase). Those relationships are consistent with the mode structures illustrated in Fig. 4, which shows one nodal line located between moorings 4 and 8 in the case of modes 1 and 2, but two nodal lines in the case of mode 3.

Spectra and intermooring comparisons of currents—More direct interpretation of the temporal and spatial structure of internal motions is provided by spectral analysis of currents. Figure 8c displays energy spectra of the v (northward) component of the current at 8 and 55 m at mooring 9 (i.e. respectively well above and well below the thermocline) and also the coherence and phase relationships of the 8- and 55-m records. The energy level is two orders of magnitude lower at 55 m than at 8. As for the temperature spectra from that mooring (Fig. 6a), the dominant feature is an energy peak near 45 h, and this is the only period band in which there is high coherence between the 8- and 55-m records. The near-180° phase relationship between 8 and 55 m confirms the opposite upper- and lower-layer current directions, again consistent with an internal wave of the first vertical mode and with a predominantly two-layered basin response. Smaller peaks near the second mode period are also evident; but no consistently spaced peaks appear at the predicted third or higher mode periods. The corresponding spectral diagrams (not illustrated) for the u (eastward) current component at mooring 9 are very similar to those displayed in Fig. 8c. This is not surprising in view of the NW/SE orientation of the Talweg at that mooring.

In an arrangement similar to that in Fig. 7b, a set of spectra of the u and v components of upper-layer currents (6 or 7 m, well above the thermocline) at a series of moorings spaced along the Talweg is assembled in Fig. 9. Most of the current spectra show energy peaks near the first and second TVD-predicted mode periods (45 and 24 h) and often a broad energy maximum centered near 100 h. Predictably, the near-45-h peaks at midbasin moorings 5 and 8 are much higher than those at moorings near the basin extremities. At mooring 1 the 45-h peak is absent in the v component and is relatively small (of about the same energy density as the near-24-h peak) at mooring 12. In spectra from all other moorings (4, 5, 8, 10 in Fig. 9, mooring 9 in Fig. 8c, and also at moorings 6 and 11, not illustrated) the near-45-h peak dominates and a near-24-h peak is usually also present. Except for pairs which include moorings 1 or 12, intermooring coherence (not illustrated) is consistent with the model-predicted structures (Fig. 4).

The square roots of the near-45-h peak heights for u and v in Fig. 9 were multiplied by 0.067 (an empirical factor obtained by analyses of test series) to yield relative speed estimates at that frequency of 0.4, 1.3, 2.5, 2.3, 0.8, and 0.7 cm s^{-1} at moorings 1, 4, 5, 8, 10, and 12, respectively. (Moorings 6 and 7 were omitted because the uppermost current meters there, at 10 and 13 m, were too near the thermocline to be representative of the upper layer.) Those estimates, when entered at the corresponding Talweg distance in figure 8b of Lemmin and Mortimer (1986), are in fair agreement with the TVDM-predicted current speeds in the case of moorings 5 and 8. Those predicted speeds, it is recalled, were those corresponding to a seiche of 100-cm maximum amplitude. We conclude from this result that the actual August–September average thermocline displacement for the first mode at the Zurich end of the basin was, in fact, near ± 100 cm. For the other moorings, the agreement between predicted and observed current speeds is less close; again the possible influence of surge passages must be considered. The surge

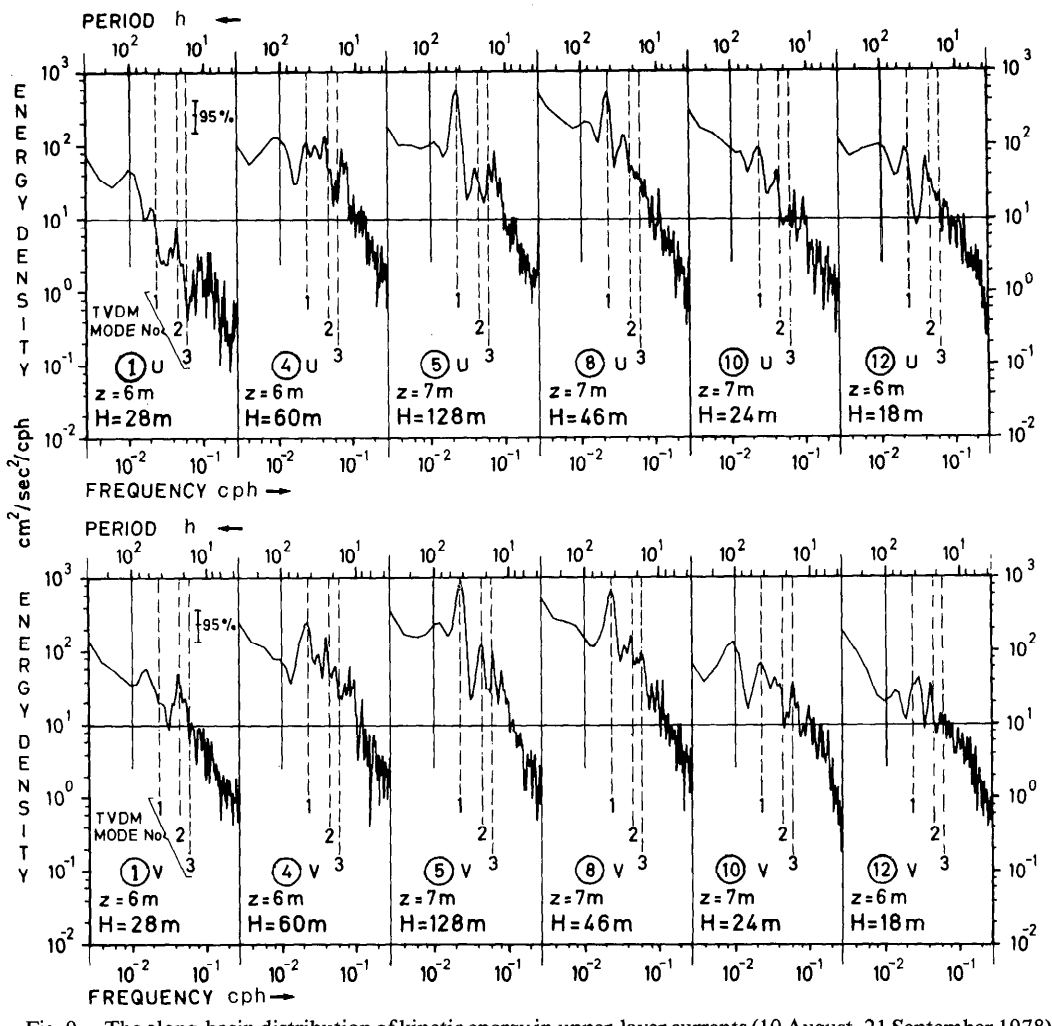

Fig. 9. The along-basin distribution of kinetic energy in upper-layer currents (10 August–21 September 1978), illustrated by spectra of the u (EW) and v (NS) components (upper and lower row) at 6- or 7-m depths at moorings 1, 4, 5, 8, 10, and 12 arranged in order along the Talweg. H denotes total water depth at the mooring.

effect on the first-mode current contribution is likely to be greater near the ends of the basin where the seiche contribution to current is small.

Observed features not reproduced by the TVDM

Rotation of current vectors—Because the internal Rossby radius of deformation approximately equaled basin width during the August–September interval, the influence of the earth's rotation on the motions considered here was not expected to be large and therefore was not taken into account in TVDM calculations. That that neglect is not entirely justified is evidenced by the Kelvin wavelike behavior sometimes seen in comparisons of temperature records from the mooring pairs 5/7 and 8/9. The main effect of rotation is to bring about transverse sloping of the interface, which generates a pressure gradient in approximate geostrophic balance with the longitudinal current, as in Loch Ness (Mortimer 1955), a basin of comparable width. Rotational effects were also sometimes seen in progressive vector

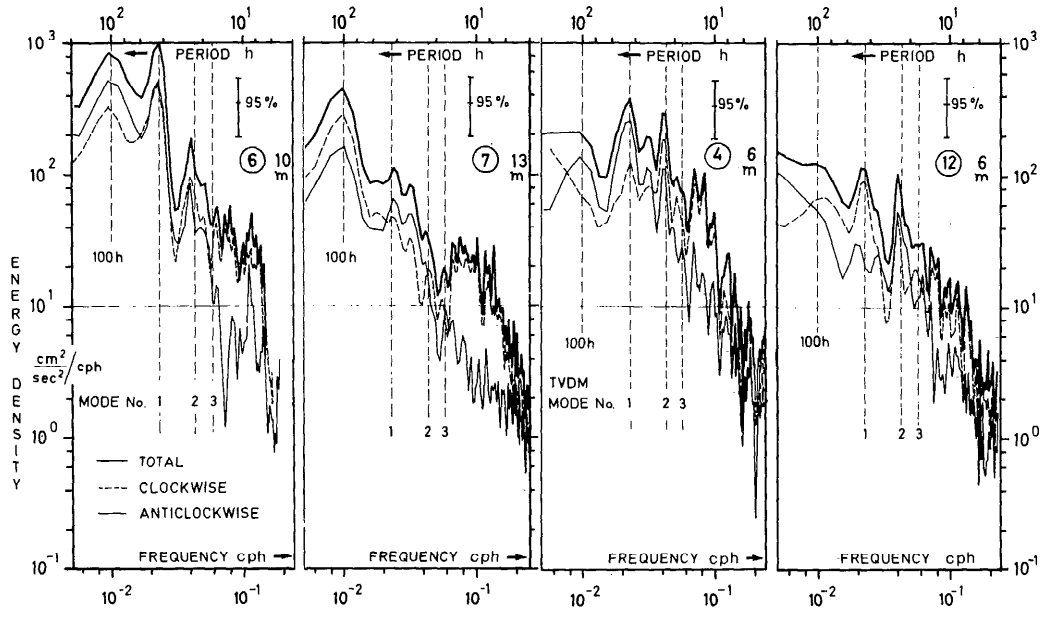

Fig. 10. Rotary spectra of current at the following moorings and depths: 6 (10 m); 7 (13 m); 4 (6 m); 12 (6 m). Total energy is indicated by the upper thick line, while the clockwise-turning and anticlockwise-turning contributions are indicated by the dashed and thin lines, respectively.

diagrams (not illustrated) prepared from current records at some of the Zurich mid-lake moorings.

Rotary features in currents can conveniently be examined by means of *rotary spectra* based on schemes developed by Gonella (1972) and Mooers (1973). These display the frequency distribution of kinetic energy partitioned into clockwise- and anticlockwise-turning currents. If, at a given frequency, the clockwise and anticlockwise contributions are equal, the *average* rotation is zero, and the average motion is therefore rectilinear. But if the partition is unbalanced, the spectra indicate the degree to which clockwise or anticlockwise rotation dominates the average behavior.

Rotary spectra of upper-layer currents were examined for all moorings. Except at moorings 6, 7, and 9 (*see Table 1*) the uppermost current meters were well above the thermocline. The evidence of rotation was variable. At most moorings (4–7, 9–12, examples in Fig. 10) clockwise rotation dominated in the period range 8 to 15 h, i.e. below the local inertial period of 16.8 h. However, energy levels were very low in that spectral region, and the apparent clockwise dominance may therefore not be real. In the region of higher energy, occupied by the 100-, 45-, and 24-h peaks, the evidence of rotation varied from mooring to mooring. No rotational effects were seen in the spectrum from mooring 1 (not illustrated). Six of the remaining nine moorings showed nearly rectilinear motion near the 45-h peak (for example 6 and 7, Fig. 10), moorings 4 and 10 predominantly anticlockwise motion, mooring 12 mostly clockwise. Near the 24-h peak, spectra from six moorings displayed nearly rectilinear motion; at moorings 4, 9, and 11 the motion was predominantly clockwise. To explain these varied results, we must take into account interactions of the Coriolis force and basin topography.

For periods above 45 h the sense of rotation was opposed at neighboring moorings 6 and 7 (Fig. 10). The probable explanation is that the current meter at mooring 7 was 13 m deep, i.e. in the thermocline region where current energy is much less than at higher levels and where there are changes in current direction as the thermocline rises and falls. Near 45 h, for example, the energy level at mooring 7 is a

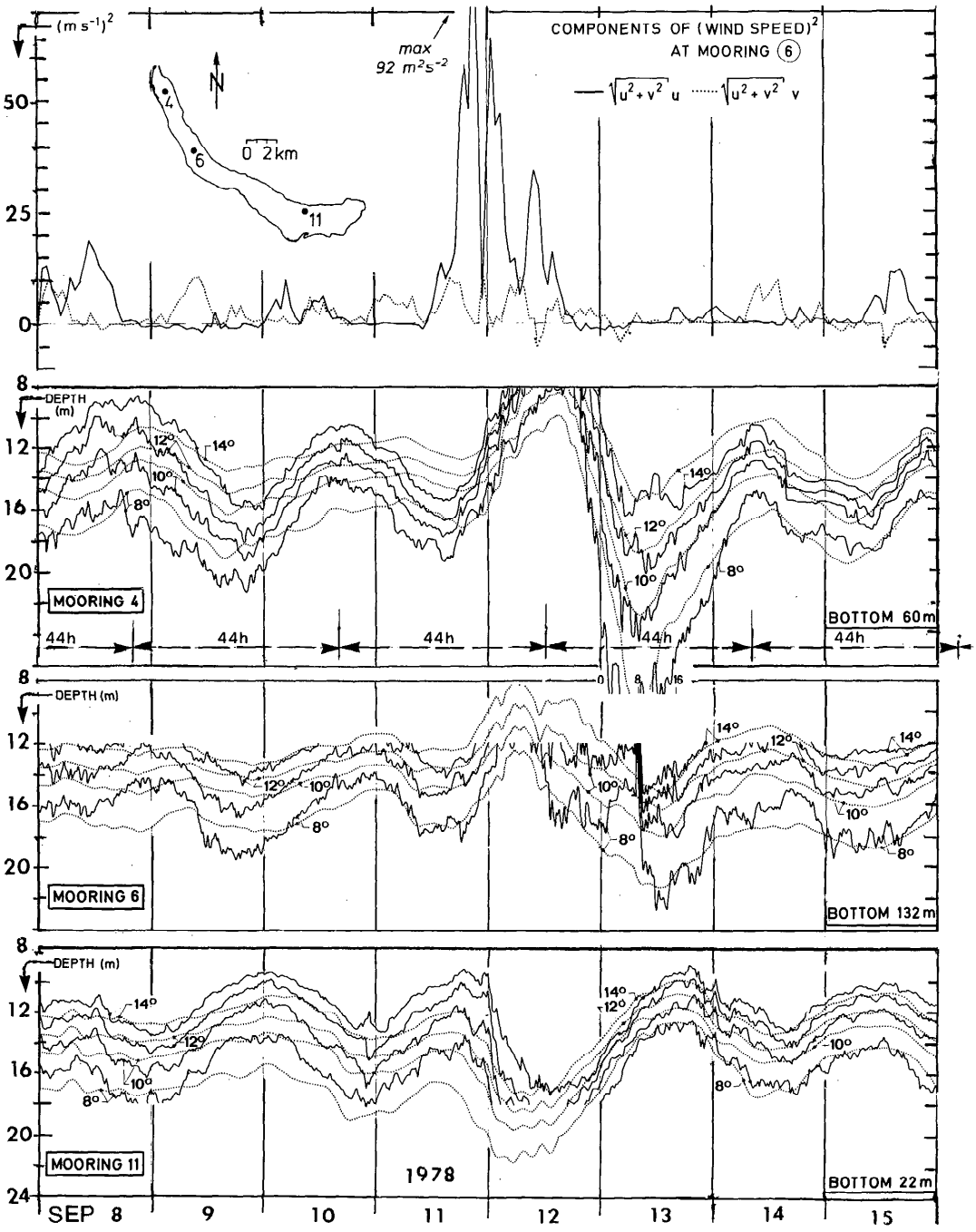

Fig. 11. Modeled and observed depth variation of the 8°, 10°, 12°, and 14°C isotherms at moorings 4, 6, and 11 from 8 to 15 September 1978. Solid lines indicate observed isotherm depths, derived from hourly averaged interpolations of temperature records at 2-m depth intervals (1-m intervals at 11; for comparable observations at moorings 9 and 10 *see* Mortimer and Horn 1982). Dotted lines are predictions of isotherm depth for the same interval from Oman's (1982) multilayer circulation model of Lake Zurich, driven by observed winds. The upper panel displays, on the same time scale, the u (EW) (solid line) and v (NS) (dotted line) components of wind speed squared 3 m above the lake surface at mooring 6.

tenth of that at 6. Near the 100-h peak the difference in energy level between moorings 6 and 7 is less, but the dominant rotation at 100 h is anticlockwise at 6, clockwise at 7. Whether this behavior (not predicted by the TVDM) must be attributed to a vorticity wave pattern remains to be explored.

Seiche-linked internal surge responses after strong wind impulses—The models we have used are based on linear theory and provide a satisfactory simulation of observed internal seiche structure as long as the amplitude of the interface deflection is not large. But when strong wind impulses generate exceptional interface deflections, the seiche takes on the character of a nonlinear wave. A steep-fronted surge develops, as described for Lake Zurich by Mortimer and Horn (1982), for Loch Ness by Mortimer (1955), and for Lake Constance by Hollan (1974, 1983). To simulate this feature we need more elaborate models which include nonlinear terms; for example the two-layer, near-resonant, wind-forced model of Thorpe (1974) or the multilayer Lake Zurich model of Oman (1982). The latter model, driven by observed winds, simulated the depth fluctuation of four selected near-thermocline isotherms (dotted lines in Fig. 11). These are compared, in the same figure, with the corresponding observed fluctuations at moorings 4, 6, and 11, over an 8-day interval that included a strong wind on 11/12 September. Part of that episode (for the 10°C isotherm only, with data for moorings 9 and 10 added) was illustrated by Mortimer and Horn (1982), with a fuller descriptive interpretation. Here we conclude, from Fig. 11, that the nonlinear, steep-fronted surge feature is satisfactorily simulated by Oman's model and that the timing of the wind impulse was such that a pre-existing 44-h seiche was reinforced. That pre-existing oscillation was approximately in phase at moorings 4 and 6 and out of phase at 11, consistent with first mode structure and period.

The large storm-produced thermocline downstroke at the Rapperswil end of the basin (mooring 11 at midnight 11/12 September) set off an internal surge, the progress of which toward Zurich could be observed at moorings along the route (Mortimer and Horn 1982). The next thermocline downstroke, this time at the Zurich end (mooring 4, just before midnight 12/13 September) generated a much larger surge, the along-basin progress and decreasing amplitude of which could also be followed through a further seiche cycle and beyond. Mortimer and Horn concluded that surges are generated at basin ends only by *downstrokes* of the thermocline and only if the downstroke is large enough to cause the internal wave to interact strongly with the bottom topography. The surge then propagates as a nonlinear progressive wave or front away from that end. Its speed of propagation may differ slightly from the phase speed of the seiche standing wave (in this example the surge speed was slightly slower); but because the surge is generated *anew* by each seiche-induced downstroke at alternating basin ends, it becomes (in that sense) phase-locked with the seiche.

Figure 11 displays the most striking example of surge generation seen during our study, but there were others. For example, in Fig. 12 the initial conditions and the timing of wind impulses were quite different from those displayed in Fig. 11. A weaker, more irregular near-44-h oscillation had been in progress (24–28 August, *see Fig. 3*), but that was apparently destroyed by the eastgoing wind impulse (1000–1200 hours on 30 August) which, on that occasion, was out of phase with the pre-existing seiche and which apparently canceled the seiche-induced depression of isotherms expected at mooring 4. At the same time the isotherms at the other end of the basin were depressed, as illustrated by the downstroke marked by A in Fig. 12 (mooring 10). That downstroke initiated a surge, the along-basin course of which is discernible at B (mooring 9), weakly at C (mooring 6), and strongly at D (mooring 4 near the Zurich end).

The downstroke at D was closely followed and reinforced by another wind impulse toward ENE at 1000 hours on 31 August, which further depressed the isotherms at mooring 4, generating a stronger downstroke and surge than would otherwise have occurred at 4. The resultant progress of that

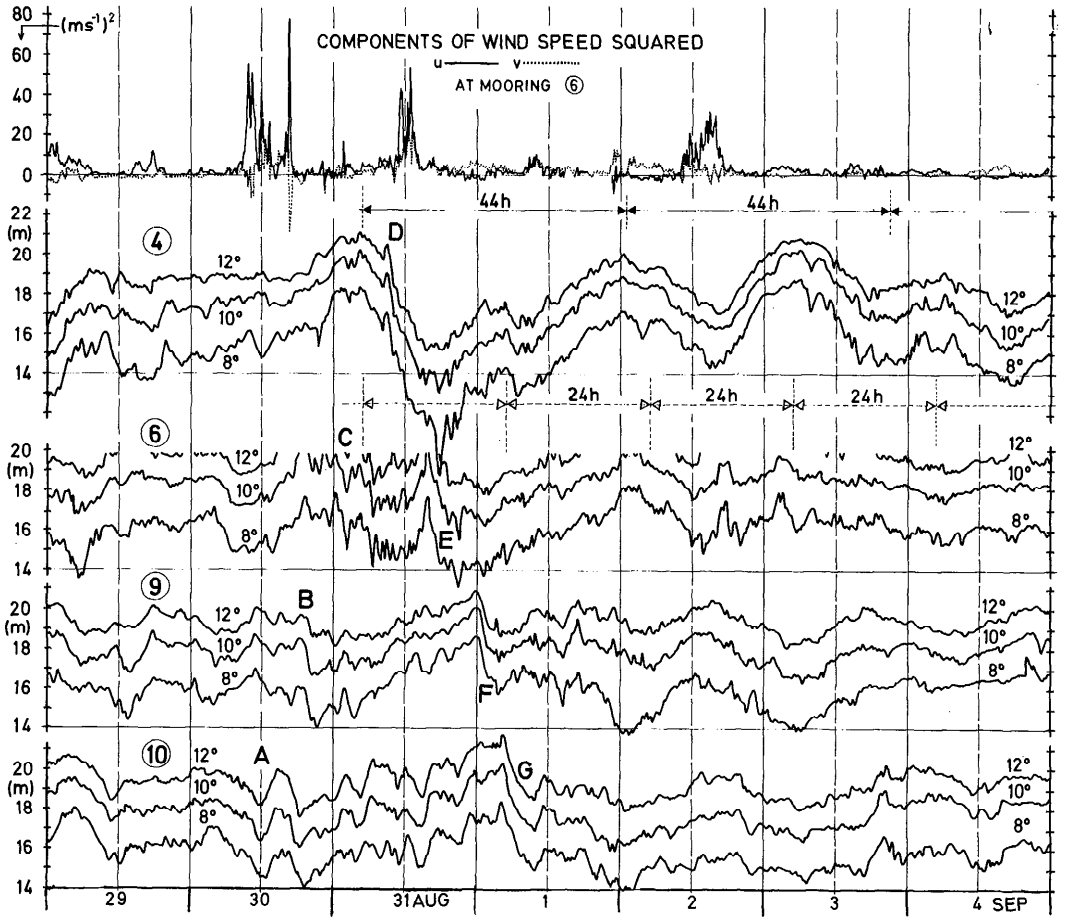

Fig. 12. Depth variation of the 8°, 10°, and 12°C isotherms at moorings 4, 6, 9, and 10, interpolated as hourly means from temperature records at 2-m depth intervals (1-m intervals at 10), 29 August–4 September 1978. Also shown (top) are the u (EW) (solid line) and v (NS) (dotted line) components of wind speed squared 3 m above the lake surface at mooring 6.

second surge can be followed during the ensuing calm period (E at 6, F at 9, and G at 10). No subsequent surge appears to have been generated at the Rapperswil end, and the lake's response to the earlier wind impulses merged into the large-amplitude internal seiche, starting at the time (0500 hours on 31 August) of maximum isotherm elevation at mooring 4. Originally that seiche contained strong first and second mode components, but following the eastgoing wind impulse during the afternoon of 2 September, the second mode became dominant and persisted (*see Fig. 3*). The timing of the wind on 2 September was apparently such that the first mode component was reduced and the second was reinforced.

Conclusions and outlook

The relatively simple models used here in an initial interpretation of the 2-month data set from stratified Lake Zurich satisfactorily reproduce the observed structures, periodicities, and phase relationships of the multimodal internal seiche responses to wind perturbations. Oscillatory responses of this type are known from (and indeed common in) other lake basins, but the comprehensive Zurich data and the spectral information derived therefrom yield insights

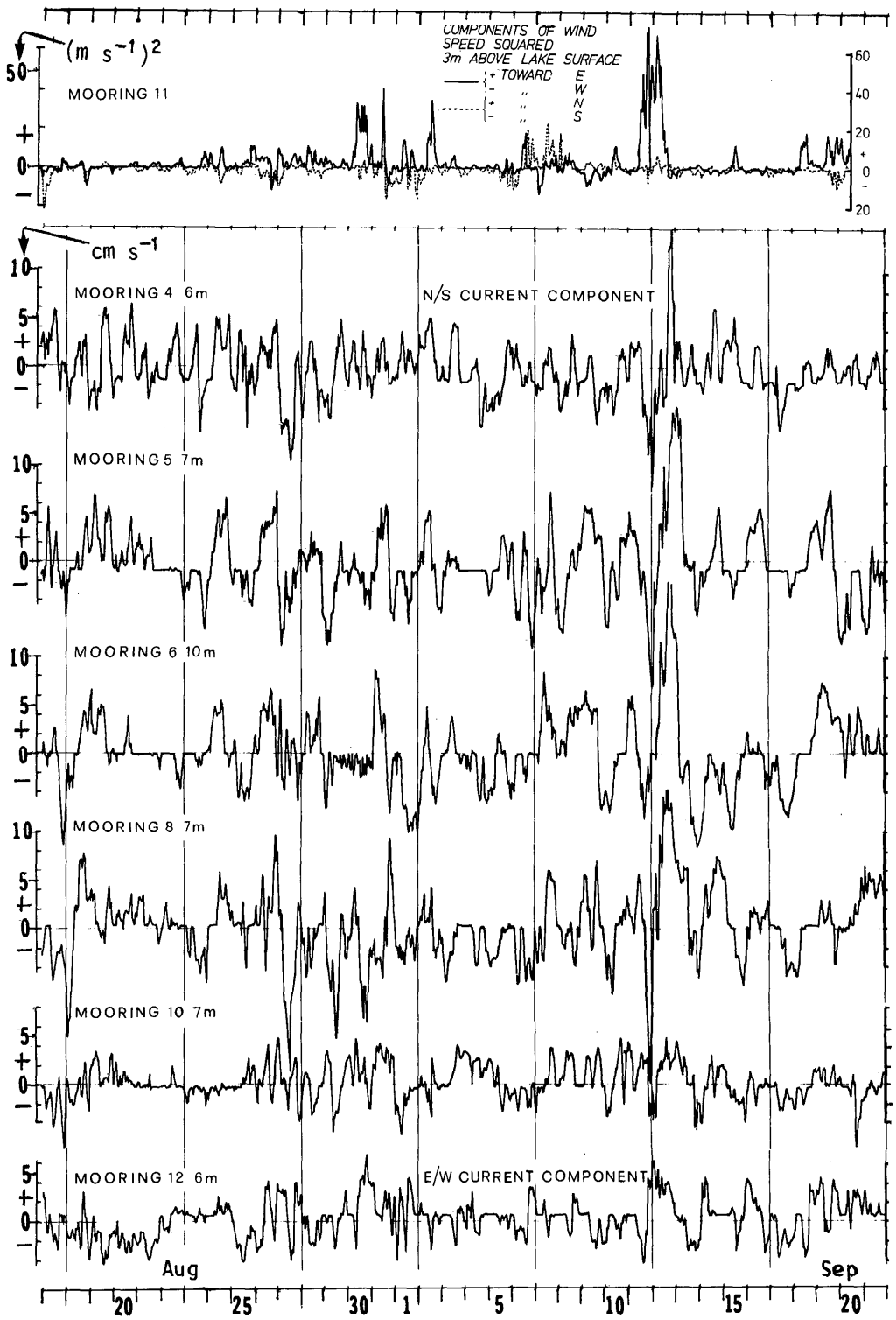
COMPONENTS OF WIND SPEED SQUARED 3m ABOVE LAKE SURFACE
+ TOWARD E
- " W
+ " N
- " S
(m s⁻¹)²
MOORING 11
cm s⁻¹
MOORING 4 6m
N/S CURRENT COMPONENT
MOORING 5 7m
MOORING 6 10m
MOORING 8 7m
MOORING 10 7m
MOORING 12 6m
E/W CURRENT COMPONENT
Aug
Sep
20
25
30
1
5
10
15
20

(in hitherto unobtainable detail) into the excitation, persistence, and decay of basin mode responses. Those responses demonstrate the control exerted by the timing, strength, and duration of winds, and also by the relative phasing of pre-existing seiche oscillations in the generation of new seiches and surges (*see Figs. 11 and 12*). Future research, perhaps exploiting these data further, will involve more complex models to address questions concerning the generation of internal seiches during the wind-forcing stage; effects of topography and the earth's rotation, perhaps leading to an explanation of the broad energy peak near 100 h in the spectra; and the nonlinear dynamics of internal surges and their reflections at basin ends.

The influence of forced and free oscillatory responses on the chemical and biological economy of the lake lies not only in the vertical and horizontal displacements of water masses, but also in the currents and turbulent mixing which they produce. That the strongest currents and associated turbulence are generated during surge passages becomes evident when the upper-layer currents are compared (Fig. 13) at six moorings along the Talweg over a time interval that includes the surge events illustrated in Figs. 11 and 12. Not surprisingly, the fastest currents were recorded after the 11/12 September storm and during the passage of the ensuing surges. At mooring 9, for example, Mortimer and Horn (1982) noted that the maximum speed at 8-m depth was 23 cm s^{-1} (SSE, hourly mean) just after the peak of the storm, while at the same time at 32 m the current was running at 9 cm s^{-1} in the opposite (NNW) direction. Acceptance of the severe simplification—that the shear was confined to and spread uniformly across a 6-m-thick thermocline (14°C at 12 m, 9°C at 18 m, density difference 6.1×10^{-4})—yields an average Richardson number of 0.35, i.e. above the limit (0.25) below which unstable flow and mixing can occur. But, recalling that the velocities used in this calculation and those illustrated in Fig. 13 are hourly means and that the shear may have been concentrated in thinner layers of the thermocline, we find it most probable that the internal surges after the 11/12 September storm (and perhaps also after the 30/31 August wind impulses) were accompanied by episodes of unstable flow and mixing within the thermocline. With nutrient depletion in the upper layer at that time of year (Thomas 1950), the biological effect of nutrient injection during the temporary opening of such a "mixing window" through the thermocline was probably significant. The frequency and the consequences of that phenomenon merit joint investigation by hydrodynamicists and biologists.

References

BLACKMAN, R. B., AND T. W. TUKEY. 1958. The measurement of power spectra. Dover.

DEFANT, A. 1918. Neue Methode zur Ermittlung der Eigenschwingungen (Seiches) von abgeschlossenen Wassermassen (Seen, Buchten, usw.). Ann. Hydrogr. Berlin **46:** 78–85.

GONELLA, T. 1972. A rotary-component method for analysing meteorological and oceanographic vector time series. Deep-Sea Res. **19:** 833–846.

HOLLAN, E. 1974. Strömungsmessungen im Bodensee. Ber. Arbeitsgem. Wasserwerke Bodensee-Rhein (AWBR) 6, p. 111–187.

———. 1983. Experiences with mathematical simulation of large scale motions in Lake Constance, Mitt. Inst. Meeresk. Univ. Hamburg 26, p. 154–198.

HORN, W. 1980. Physikalisch-limnologische Untersuchungen in Schweizer Seen. Wasser, Energie, Luft 1980 (9), p. 276–284.

HUTTER, K., G. SALVADÉ, AND D. J. SCHWAB. 1983. On internal wave dynamics in the northern basin of the Lake of Lugano. Geophys. Astrophys. Fluid Dyn. **27:** 299–336.

JENKINS, G. M., AND D. W. WATTS. 1968. Spectral analysis and its applications. Holden-Day.

LAMMEL, K. 1984. Der geschichtete Kochelsee unter Windlast: Erste Datenauswertung und Ergebnisse. Dtsch. Gewaesserkd. Mitt. 28, p. 44–49.

LEMMIN, U., AND C. H. MORTIMER. 1986. Tests of an extension to internal seiches of Defant's procedure for determination of surface seiche char-

←

Fig. 13. Hourly mean speeds of the *v* (NS) component of current in the upper layer observed at moorings 4, 5, 6, 8, and 10 (and *u* component at mooring 12) 17 August–21 September 1978 (extracted from data report of W. Horn, *see Fig. 2 legend*). Top panel, as Fig. 12 but at mooring 11.

acteristics in real lakes. Limnol. Oceanogr. **31:** 1207–1231.

MOOERS, C. N. 1973. A technique for cross spectrum analysis of pairs of complex-valued time series with emphasis on properties of polarized components and rotational invariants. Deep-Sea Res. **20:** 1129–1141.

MORTIMER, C. H. 1953. The resonant response of stratified lakes to wind. Schweiz. Z. Hydrol. **15:** 94–151.

———. 1955. Some effects of the earth's rotation on water movements in stratified lakes. Int. Ver. Theor. Angew. Limnol. Verh. **12:** 66–77.

———. 1979. Strategies for coupling data collection and analysis with dynamic modelling of lake motions, p. 183–277. *In* Lake hydrodynamics. Symp. Proc. Elsevier.

———, AND E. J. FEE. 1976. Free surface oscillations and tides of Lakes Michigan and Superior. Phil. Trans. R. Soc. Lond. Ser. A **281:** 1–61.

———, AND W. HORN. 1982. Internal wave dynamics and their implications for plankton biology in the Lake of Zurich. Vierteljahresschr. Naturforsch. Ges. Zuerich **137:** 299–318.

MYSAK, L. A., G. SALVADE, K. HUTTER, AND T. SCHEIWILLER. 1985. Topographic waves in an elliptical basin, with application to the Lake of Lugano. Phil. Trans. R. Soc. Lond. Ser. A **316:** 1–55.

OMAN, G. 1982. Das Verhalten des geschichteten Zürichsees unter ausseren Windlasten. Versuchsanst. Wasserbau Hydrol. Glaziol. Eidg. Tech. Hochsch. Zuerich Mitt. 60.

PHILLIPS, O. M. 1971. On spectra measured in an undulating layered medium. J. Phys. Oceanogr. **1:** 1–6.

SAYLOR, J. H., J. C. HUANG, AND R. O. REID. 1980. Vortex modes in southern Lake Michigan. J. Phys. Oceanogr. **10:** 1814–1823.

SCHWAB, D. J. 1977. Internal free oscillations in Lake Ontario. Limnol. Oceanogr. **22:** 700–708.

SMITH, B. T., AND OTHERS. 1974. Matrix eigensystem routines–Eispack guides. *In* G. Goos and J. Hartmanis [eds.], Lecture notes in computer science. V. 6. Springer.

STOCKER, T., AND K. HUTTER. 1985. A model for topographic Rossby waves in channels and lakes. Versuchsanst. Wasserbau Hydrol. Glaziol. Eidg. Tech. Hochsch. Zuerich Mitt. 76. [*also* in press: J. Fluid Mech.]

THOMAS, E. A. 1949. Sprungschichtneigung im Zürichsee durch Sturm. Schweiz. Z. Hydrol. **11:** 527–545.

———. 1950. Auffällige biologische Folgen von Sprungschichtneigungen im Zürichsee. Schweiz. Z. Hydrol. **12:** 5–23.

THORPE, S. A. 1974. Near-resonant forcing in a shallow two-layer fluid: A model for the internal surge in Loch Ness? J. Fluid Mech. **63:** 509–527.

Submitted: 30 December 1985
Accepted: 19 May 1986